EC
Journals.ASM.org

Interaction Maps of the *Saccharomyces cerevisiae* ESCRT-III Protein Snf7

Barbara Sciskala, Ralf Kölling

Institut für Lebensmittelwissenschaft und Biotechnologie, Fg. Gärungstechnologie, Universität Hohenheim, Stuttgart, Germany

The *Saccharomyces cerevisiae* ESCRT-III protein Snf7 is part of an intricate interaction network at the endosomal membrane. Interaction maps of Snf7 were established by measuring the degree of binding of individual binding partners to putative binding motifs along the Snf7 sequence by glutathione *S*-transferase (GST) pulldown. For each interaction partner, distinct binding profiles were obtained. The following observations were made. The ESCRT-III subunits Vps20 and Vps24 showed a complementary binding pattern, suggesting a model for the series of events in the ESCRT-III functional cycle. Vps4 bound to individual Snf7 motifs but not to full-length Snf7. This suggests that Vps4 does not bind to the closed conformation of Snf7. We also demonstrate for the first time that the ALIX/Bro1 homologue Rim20 binds to the α6 helix of Snf7. Analysis of a Snf7 α6 deletion mutant showed that the α6 helix is crucial for binding of Bro1 and Rim20 *in vivo* and is indispensable for the multivesicular body (MVB)-sorting and Rim-signaling functions of Snf7. The Snf7Δα6 protein still appeared to be incorporated into ESCRT-III complexes at the endosomal membrane, but disassembly of the complex seemed to be defective. In summary, our study argues against the view that the ESCRT cycle is governed by single one-to-one interactions between individual components and emphasizes the network character of the ESCRT interactions.

The *Saccharomyces cerevisiae* endocytic pathway consists of several distinct endocytic compartments, which can be distinguished by their morphology and the presence of marker proteins (1). Internalized cell surface proteins first enter early endosomes, a central sorting station, where proteins destined for degradation are separated from proteins that are recycled back to the cell surface (2). The early endosome then matures into a late endosome or multivesicular body (MVB) by the formation of vesicles that bud into the interior of the late endosome (3). Cargo for the degradative pathway is sorted into these internal vesicles (ILVs).

A set of proteins, the "endosomal sorting complex required for transport" (ESCRT) proteins, is required for cargo recruitment and ILV formation. These proteins can be grouped into several protein complexes (ESCRT-0, -I, -II, and -III and the Vps4 ATPase complex) that are thought to act consecutively in the process of cargo recruitment and vesicle formation (4). The ESCRT-III complex appears to be crucial for the final stage of ILV formation, the membrane abscission step (5, 6). Yeast ESCRT-III is composed of four proteins (Snf7, Vps20, Vps2/Did4, and Vps24) (7) that are part of a protein family consisting of six proteins in yeast (8, 9). The other two members of the protein family that are not considered part of ESCRT-III (Mos10/Vps60 and Did2) are closely associated with ESCRT-III function (9, 10). The different subunits are not present in equimolar amounts in the complex: Snf7 seems to be the most important and most abundant protein of the complex, while the other subunits and associated proteins appear rather to play a more regulatory role (11, 12). Vps20 is important for Snf7 membrane recruitment and promotes Snf7 oligomerization. Vps24 in association with Vps2 in turn restricts Snf7 oligomerization by capping the Snf7 oligomer and recruiting the AAA-ATPase Vps4 to the complex for disassembly.

Biochemical as well as two-hybrid data indicate that Snf7 directly binds to Vps20, Vps24, and Vps4 (11, 13, 14). Vps4 binds to ESCRT-III proteins via its N-terminal MIT (microtubule interacting and transport) domain (15, 16). It recognizes two different motifs on ESCRT-III proteins, the MIM1 motif found at the C terminus of Vps2 and Did2 (15, 16) and the MIM2 motif found in the C-terminal regions of Snf7 and Vps20 (17). The two motifs bind to distinct surfaces of the MIT domain.

Other proteins are also thought to interact with Snf7. Evidence has been presented that the yeast orthologue of human ALIX, Bro1, binds to the C terminus of Snf7 (5). Bro1 recruits the deubiquitinating enzyme (DUB) Doa4 to late endosomes, where it removes ubiquitin from endocytic cargo proteins before their incorporation into ILVs. Bro1 binding is required for DUB activity of Doa4 (18). In addition, Bro1 appears to play a Doa4-independent role late in MVB sorting (19). Another potential binding partner of Snf7 is Vta1, which forms a complex with Vps4 (20). However, interaction has been demonstrated only by two-hybrid analysis so far (13).

The ESCRT network is closely linked to signaling events that affect gene expression in the nucleus. Most ESCRT functions "upstream" of Snf7 are required for the induction of the Rim pathway (21–24), which is activated by a shift to an alkaline pH. Activation of the Rim pathway leads to processing of the transcription factor Rim101 to its active form (25). It is thought that Rim101 processing occurs at endosomes and that Snf7 serves as a platform for recruitment of the factors required for Rim101 processing. Accordingly, the functions of the ESCRT proteins in Rim signaling would be to bring Snf7 to the endosomal membrane. There is evidence that the Rim proteins Rim13, Rim20, and Ygr122w bind to Snf7 (13, 26–28). The Rim functions are not required for MVB sorting.

Received 11 September 2013 **Accepted** 11 September 2013
Published ahead of print 20 September 2013
Address correspondence to Ralf Kölling, ralf.koelling@uni-hohenheim.de.

doi:10.1128/EC.00241-13

TABLE 1 Yeast strains

Strain	Genotype	Reference
JD52	*MAT***a** *his3-Δ200 leu2-3,112 lys2-801 trp1-Δ63 ura3-52*	J. Dohmen, Cologne, Germany
RKY1633	*VPS20-13myc*::*HIS3*	27
RKY1949	*YGR122w-13myc*::*HIS3*	This study
RKY2029	*BRO1-13myc*::*kanMX*	27
RKY2030	*BRO1-13myc*::*kanMX Δsnf7*::*TRP1*	27
RKY2097	*RIM20-13myc*::*kanMX Δsnf7*::*TRP1*	27
RKY2099	*RIM20-13myc*::*kanMX*	27
RKY2106	*RIM13-13myc*::*kanMX*	27
RKY2175	*Δrim101*::*HIS3*	27
RKY2402	*VPS4-13myc*::*HIS3*	27
RKY2419	*VPS24-13myc*::*HIS3*	This study
RKY2530	*VTA1-13myc*::*kanMX*	This study
RKY2673	*Δsnf7*::*kanMX*	This study

To extend our knowledge about this complex network of interactions, our goal was to establish an interaction map of Snf7 with its various interaction partners. We found that Vps20 and Vps24 interact with Snf7 in a complementary fashion. The pattern of interactions suggests a model for the order of events during an assembly/disassembly cycle of the ESCRT complexes at the endosomal membrane. Furthermore, we demonstrate for the first time that Rim20 interacts with the C-terminal α-helix of Snf7. Our experiments show that the C-terminal α-helix is essential for the MVB sorting function and for Rim signaling.

MATERIALS AND METHODS

Strains and plasmids. Yeast cells were grown either in YPD medium (1% yeast extract, 2% Bacto peptone, 2% glucose) or in SD/CAS medium (0.67% yeast nitrogen base, 1% Casamino Acids, 2% glucose) to select for the presence of plasmids (with the *URA3* or *TRP1* marker). All yeast strains (Table 1) are derived from JD52. The 13myc coding sequence was introduced into the yeast genome at the 3′ ends of the corresponding genes by a double crossover with PCR-generated cassettes (29). The integration was verified by PCR with specific primers. The *SNF7* gene was deleted similarly. The vector plasmid pRK1235 was derived from pGEX-3X (GE Healthcare, Freiburg, Germany) by insertion of a SalI linker into the EcoRI site. For construction of glutathione *S*-transferase (GST) fusions, a pair of annealed linker oligonucleotides with BamHI and SalI overhangs was inserted into pRK1235 cut with BamHI and SalI. The amino acids encoded by these linkers are listed in Table 2. The *Escherichia coli* strain used for the expression of GST fusions was XL-1 Blue (Agilent Technologies, Waldbronn, Germany). To construct pRK861, a *SNF7* PCR fragment with JD52 as the template was cloned into YCplac33. A 5′-truncated version of *SNF7* was cloned into YCplac33 to give pRK1487. This plasmid also contains a *CYC1* terminator fragment downstream of the *snf7Δα6* gene.

GST pulldown. Prewarmed LB medium (200 ml, containing 50 μg/ml ampicillin) was inoculated with 20 ml overnight culture of *E. coli* XL-1 Blue transformed with the GST fusion expression plasmids and grown for 1 h at 37°C. The culture was cooled to room temperature on ice, and 1 mM isopropyl-ß-D-thiogalactopyranoside (IPTG) was added to induce expression of the GST fusion proteins. After 4 h of incubation at 25°C, 20 OD_{600} (optical density at 600 nm) units of cells were harvested (1 OD_{600} unit = 5×10^7 cells/ml) and washed in 5 ml cold phosphate-buffered saline (PBS) buffer. The cell pellet was resuspended in 200 μl cold lysis buffer (PBS containing 1% Triton X-100 and protease inhibitor cocktail), and the cells were lysed by vortexing with glass beads (diameter, 0.1 mm) for 5 min at 4°C. After addition of 500 μl lysis buffer (total volume, 750 μl), the cell lysate was spun at 13,000 × *g* for 10 min at 4°C. A 100-μl portion of the cleared cell lysate was mixed with 100 μl 50% glutathione-Sepharose bead slurry in PBS (GE Healthcare, Freiburg, Germany) and incubated for 30 min at room temperature on a rocker. Then 100 μl of cleared yeast cell extract from cells expressing 13myc-tagged proteins was added. Yeast cell extracts were prepared essentially as described above for the *E. coli* cell extracts, with the exceptions that the yeast cultures were grown for 4 h in YPD medium at 30°C and that larger glass beads were used for cell lysis (diameter, 0.4 mm). The glutathione beads were incubated with the yeast cell extracts for 1 h at 4°C. Then the beads were washed 4 times with 1 ml cold PBS (500 × *g* spin for 1 min). Bound proteins were eluted from the beads by incubation in 100 μl sample buffer for 5 min at 95°C and separated on SDS-PAGE gels. The GST fusions were visualized by Coomassie staining, and bound yeast proteins were detected by Western blotting with anti-Myc antibodies.

Coimmunoprecipitation. Exponentially growing cells (10 OD_{600} units; $OD_{600} < 1.0$, 5×10^7 cells/ml) in SD/CAS medium were harvested, washed in 10 mM NaN_3, resuspended in 200 μl immunoprecipitation (IP) buffer (100 mM NaCl, 3 mM $MgCl_2$, 50 mM Tris-Cl [pH 7.5], 5% glycerol, and 1% Triton X-100 plus protease inhibitor cocktail), and lysed by agitation with glass beads for 5 min. After addition of 500 μl of IP buffer, samples were incubated on ice for 30 min for membrane solubilization. Then the cell extracts were centrifuged for 5 min at 500 × *g* to remove cell debris. The supernatant was incubated for 1 h at 4°C with anti-Myc antibody and for another 1 h at 4°C with 50 μl protein A-Sepharose beads (20% suspension). The protein A beads were washed three times with IP buffer in a tabletop centrifuge (twice for 1 min at 150 × *g* and once for 20 s at 13,000 × *g*), resuspended in 100 μl SDS gel sample buffer, and incubated for 5 min at 95°C before gel loading.

Differential centrifugation. Exponentially growing cells (10 OD_{600} units; $OD_{600} < 1.0$, 5×10^7 cells/ml) in SD/CAS medium were harvested, washed in 10 mM NaN_3, and resuspended in 200 μl lysis buffer (0.3 M sorbitol, 50 mM HEPES [pH 7.5], and 10 mM NaN_3 plus protease inhibitor cocktail). Cells were lysed by vortexing with glass beads for 5 min at

TABLE 2 Snf7 sequence motifs

Motif	Sequence[a]	Reference(s)
Nterm	1 MWSSLFGWTSSN	
α4	120 GLDIDKVDETMDEIREQVELGDEISDAISRP	
α5	157 EVDEDELDEELDMLAQENANQ	
MIM2	197 VSLPSVPSNKIKQS	
α6	225 DEDEKALRELQAEMGL	
Binding motifs		
MIM1	D/E-X-X-L-X-X-R-L-X-X-L-K/R	15, 16
MIM2	Φ-D/E-L-P-D/E-V-P-S-D/E-L-P	17
Alix binding	M/L/I-X-X-L-X-X-W	31

[a] Numbers are the positions of the first residue in the Snf7 sequence. The bottom three sequences are consensus sequences. Φ, aliphatic residue.

4°C. After addition of 700 μl lysis buffer, intact cells and cell debris were removed by centrifugation at 500 × *g* for 5 min. The cleared cell extract was first spun at 13,000 × *g* for 10 min to give the P13 pellet fraction and the S13 supernatant. The S13 fraction was then centrifuged at 100,000 × *g* for 1 h to give the P100 pellet and the S100 supernatant. To test for detergent solubility, half of the extract was treated with 1% Triton X-100 for 30 min on ice before centrifugation. Equal portions of the fractions were assayed for the presence of proteins by Western blotting.

Flotation gradients. Exponentially growing cells (20 OD_{600} units; $OD_{600} < 1.0$, 5×10^7 cells/ml) in SD/CAS medium were harvested, washed in 10 mM NaN_3, and lysed by agitation with glass beads in TNE buffer (50 mM Tris [pH 7.4], 150 mM NaCl, and 5 mM EDTA plus protease inhibitors). After removal of cell debris and intact cells by centrifugation at 500 × *g* for 5 min, 175 μl of cleared cell extract were mixed with 350 μl of 60% Optiprep solution (Axis-Shield, Oslo, Norway). The resulting 40% Optiprep fraction was transferred to the bottom of a centrifugation tube and overlaid with 840 μl 30% Optiprep in TNE buffer and 140 μl TNE. The gradients were centrifuged at 100,000 × *g* for 2 h at 4°C. Six equal fractions were collected and assayed for the presence of proteins by Western blotting.

RESULTS

Snf7 is part of an intricate interaction network at the endosomal membrane. Although much information has been gained about the structure of individual complexes, the dynamics of the interactions is still poorly understood. By means of both high- and low-throughput studies, many interaction partners of Snf7 have been identified, but until now, only a few interactions had been studied in detail. Here, we wanted to identify the regions within Snf7 that are engaged in the interaction with its various binding partners.

The three-dimensional (3D) structure has been solved for human CHMP3, the yeast orthologue of Vps24, and it is assumed that the overall structure is similar for all ESCRT-III proteins (30). The CHMP3 core structure consists of a four-helix bundle, with two long helices (α1 and α2) forming a 70-Å hairpin structure and two additional short helices (α3 and α4) across the α1-α2 hairpin. A fifth helix (α5) is connected to the core by a largely disordered linker, and a sixth, C-terminal helix (α6) is not represented in the structure. Putative binding motifs were suggested by previous studies with other ESCRT-III proteins in yeast and in mammalian cells (15–17); in particular, the α-helical segments in the C-terminal half of Snf7 seemed to be promising candidates. Therefore, we selected the following motifs for our analysis: the helices α4, α5, and α6, a putative MIM2 motif between helix α5 and α6, and the N-terminal region, resembling the ALIX/Bro1 binding motif of the human Snf7 orthologue CHMP4 (31) (Table 2).

The interactions were studied by GST pulldown. GST fusions with the putative binding motifs at the C-terminal end were expressed in *E. coli* to high levels. As controls, we used GST fused to full-length Snf7 and GST without a fusion partner. The GST fusions were purified from *E. coli* cell extracts with glutathione beads (Fig. 1). The beads with the bound fusion proteins were mixed with yeast cell extracts expressing the putative Snf7 interaction partners marked with a 13myc tag at the C-terminal end. After washing of the beads, bound complexes were eluted from the beads and analyzed by Western blotting with anti-Myc antibodies (Fig. 2). A quantification of the Western blot signals is depicted in Fig. 3. Two independent sets of experiments were performed, presented in two separate columns for each GST fusion in Fig. 3, together with the average of the two experiments with standard deviations. The two experiments were in excellent agreement with each other. No binding signal was detected with GST alone.

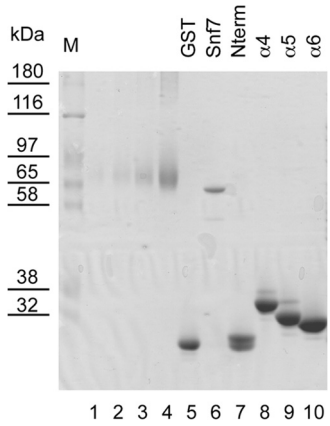

FIG 1 Purification of GST fusions from *E. coli*. GST fused to Snf7 fragments was purified with glutathione-Sepharose beads from cell extracts of *E. coli* XL-1 Blue transformed with GST fusion expression plasmids. The amount of protein corresponding to 1 OD_{600} unit of cells was run on an SDS-PAGE gel and stained with Coomassie blue. The following plasmids were used: pGEX-3X (vector) (lane 5), pRK908 (full-length Snf7) (lane 6), pRK1273 (Nterm) (lane 7), pRK1274 (α4) (lane 8), pRK1275 (α5) (lane 9), and pRK1276 (α6) (lane 10). Lanes 1 to 4 contain bovine serum albumin standards (0.1, 1, 2, and 5 μg). M, prestained protein marker. (MIM2 was expressed to comparable levels from plasmid pRK1277 [not shown].).

In all cases, except for Rim13, where we could not detect binding to any of the Snf7 fragments, a specific binding profile was observed. The profiles were quite distinct for the different interaction partners. This is especially obvious for the ESCRT-III subunits Vps20 and Vps24, which show a complementary pattern of interactions. While Vps24 interacted mainly with α4 and α5, Vps20 showed a strong interaction with the C-terminal motifs MIM2 and α6, in addition to an α4 interaction.

Vps4 and Vta1 are part of a double-ring structure and act downstream of ESCRT-III (20). Although these two interaction partners bound to all Snf7 fragments, they showed a clear preference for the MIM2 sequence. This confirms earlier findings that the putative MIM2 motif in Snf7 is relevant for Vps4 (or Vta1) binding (14). A remarkable difference was observed in the binding to full-length Snf7 versus binding to Snf7 fragments. While robust binding of full-length Snf7 was seen with Vta1, Vps4 hardly bound to full-length Snf7. This could reflect a conformation sensitivity of binding of the two proteins.

Surprisingly, the three yeast Bro domain proteins (Bro1, Rim20, and Ygr122w) differed in their binding profiles. It has been reported that Bro1 binds to the Snf7 α6 helix (5). Thus, for all three Bro domain proteins, a preference for α6 would have been expected. However, for Bro1, only a slight (but significant) preference for α6 could be detected, and Ygr122w bound more or less equally to all fragments, with a slight preference for α4. For Rim20, the situation was completely different: this protein almost exclusively bound to α6. This is the first report defining the Rim20 binding motif in Snf7.

To further explore the role of the α6 helix of Snf7 in MVB sorting and Rim signaling, we generated a *snf7*Δα*6* deletion mutant, where the last 12 codons of the *SNF7* gene (coding for the α6 helix) were deleted. Since α6 appears to be a major binding site for the Bro domain proteins Bro1 (5) and Rim20 (this study), we first

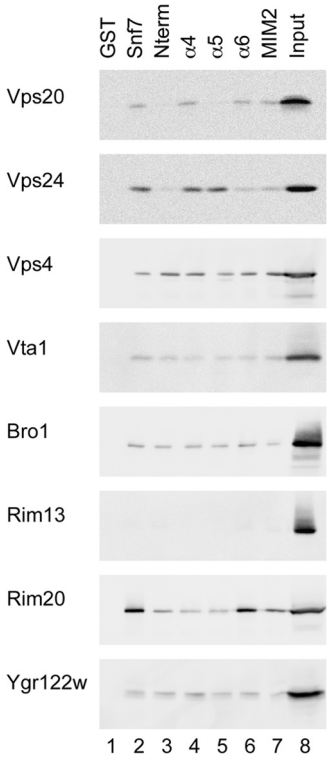

FIG 2 GST pulldown. Yeast cell extracts of strains expressing 13myc-tagged Snf7 binding partners were incubated with GST-Snf7 fusions bound to glutathione beads. Bound proteins were eluted from the beads and examined by Western blotting with anti-Myc antibodies. The following yeast strains were used (top to bottom): RKY1633 (Vps20-13myc), RKY2419 (Vps24-13myc), RKY2402 (Vps4-13myc), RKY2530 (Vta1-13myc), RKY2029 (Bro1-13myc), RKY2106 (Rim13-13myc), RKY2099 (Rim20-13myc), and RKY1949 (Ygr122w-13myc). Yeast cell extracts corresponding to 1.5 OD_{600} of cells were used in each experiment. As an input control (lane 8), total yeast cell extract from 0.2 OD_{600} unit of cells was loaded onto the gel. The GST fusions were purified from XL-1 Blue transformed with the following plasmids: pGEX-3X (lane 1), pRK908 (full-length Snf7) (lane 2), pRK1273 (Nterm) (lane 3), pRK1274 (α4) (lane 4), pRK1275 (α5) (lane 5), pRK1276 (α6) (lane 6), and pRK1277 (MIM2) (lane 7). GST fusions corresponding to 1.5 OD_{600} units of cells were used in each assay. The GST fusions were present in large excess (5 to 20 μg) over the 13myc-tagged binding partners in the yeast cell extract (in the nanogram range).

examined whether the deletion affects Snf7 binding to these proteins *in vivo*. To this end, single-copy plasmids expressing wild-type Snf7 or Snf7Δα6 were introduced into *SNF7* deletion strains expressing tagged versions of Bro1 and Rim20. The C-terminally 13myc-tagged proteins were immunoprecipitated from cell extracts, and the precipitates were analyzed for the presence of coimmunoprecipitated Snf7. As noted before, both proteins were able to precipitate wild-type Snf7, but no coimmunoprecipitation of Snf7Δα6 was observed with either protein (Fig. 4). Thus, the α6 helix of Snf7 appears to be crucial for Bro1 and Rim20 binding *in vivo*.

Next, we examined the functional consequences of the α6 deletion. To assess the impact of the α6 deletion on MVB sorting, we measured the turnover of the **a**-factor transporter Ste6, which is a cargo protein for the MVB pathway. Ste6 is transported to the cell surface but is rapidly internalized by endocytosis and is then transported to the yeast vacuole for degradation via the MVB pathway. Under normal conditions, the half-life of the protein is very short, but in ESCRT mutants, like the Δ*snf7* mutant, the protein is strongly stabilized, since transport to the vacuole is blocked in these mutants. Ste6 turnover was analyzed by a Gal depletion experiment. A *SNF7* deletion strain was transformed with a vector plasmid or with plasmids expressing either wild-type Snf7 or Snf7Δα6 and an additional plasmid expressing Myc-tagged Ste6 from the *GAL1* promoter. The cells were first grown on galactose medium to induce expression of *STE6* and were then transferred to glucose-containing medium to repress transcription of the gene. As expected, Ste6 was quickly degraded in the strain expressing wild-type Snf7 and was strongly stabilized in the vector control expressing no Snf7 (Fig. 5). The strain expressing Snf7Δα6 behaved like a complete knockout, in that Ste6 was just as stable as in the Δ*snf7* situation. Thus, the α6 helix is indispensable for the MVB-sorting function of Snf7.

Snf7 together with most of the ESCRT machinery is also required for Rim signaling. We therefore asked whether the α6 deletion affects this process. One of the *rim* phenotypes is increased sensitivity to lithium ions. To test for this phenotype, serial dilutions of different cultures were spotted onto rich-medium plates with and without 0.3 M LiCl. As expected, the wild-type strain formed colonies on the LiCl plates, while the *RIM101* deletion strain was not able to grow (Fig. 6). Likewise, the Δ*snf7* strain transformed with the empty vector could not grow on these plates. This defect was complemented by wild-type *SNF7* but not by *snf7*Δα6. Thus, the α6 helix is also indispensable for the Rim-signaling function of Snf7.

So far, *snf7*Δα6 had behaved as a complete knockout with respect to MVB sorting and Rim signaling. We wondered whether the Snf7α6 protein was completely nonfunctional or whether it retained some of the Snf7 functions. Therefore, we examined by differential centrifugation whether the mutant protein could still be recruited to endosomal membranes. About one-third of wild-type Snf7 was found in the P13 and P100 pellet fractions, while about two-thirds of the protein was soluble (Fig. 7). To prove that the pelletable fraction indeed corresponds to membrane-associated protein and not simply to large protein complexes or protein aggregates, the protein fractions were tested for their Triton X-100 solubility. If Snf7 associates with membranes, it should be shifted from the pellet fractions to the soluble fraction upon Triton X-100 treatment. Indeed, Triton X-100 solubilized about two-thirds of the protein present in the P13 pellet. Part of the P13 fraction and the complete P100 fraction, however, were detergent resistant. This protein fraction could correspond to large protein complexes (e.g., filaments), or it could be associated with detergent-resistant membranes (DRMs; also called rafts). From this experiment, we conclude that at least 15% of wild-type Snf7 is membrane associated under these conditions. Similar findings have been reported previously (7). For Snf7Δα6, a strikingly different pattern was observed (Fig. 7). Here, about 90% of the protein was found in the pellet fractions. Most of the protein present in the P13 fraction could be solubilized by Triton X-100, indicative of membrane association. Again, the P100 fraction proved to be detergent resistant. From this experiment, we conclude that about 60% of Snf7Δα6 is membrane associated.

As an alternative way to prove membrane association of Snf7, we performed a flotation experiment. In this experiment, yeast cell extracts were overlaid with different concentrations of Optiprep

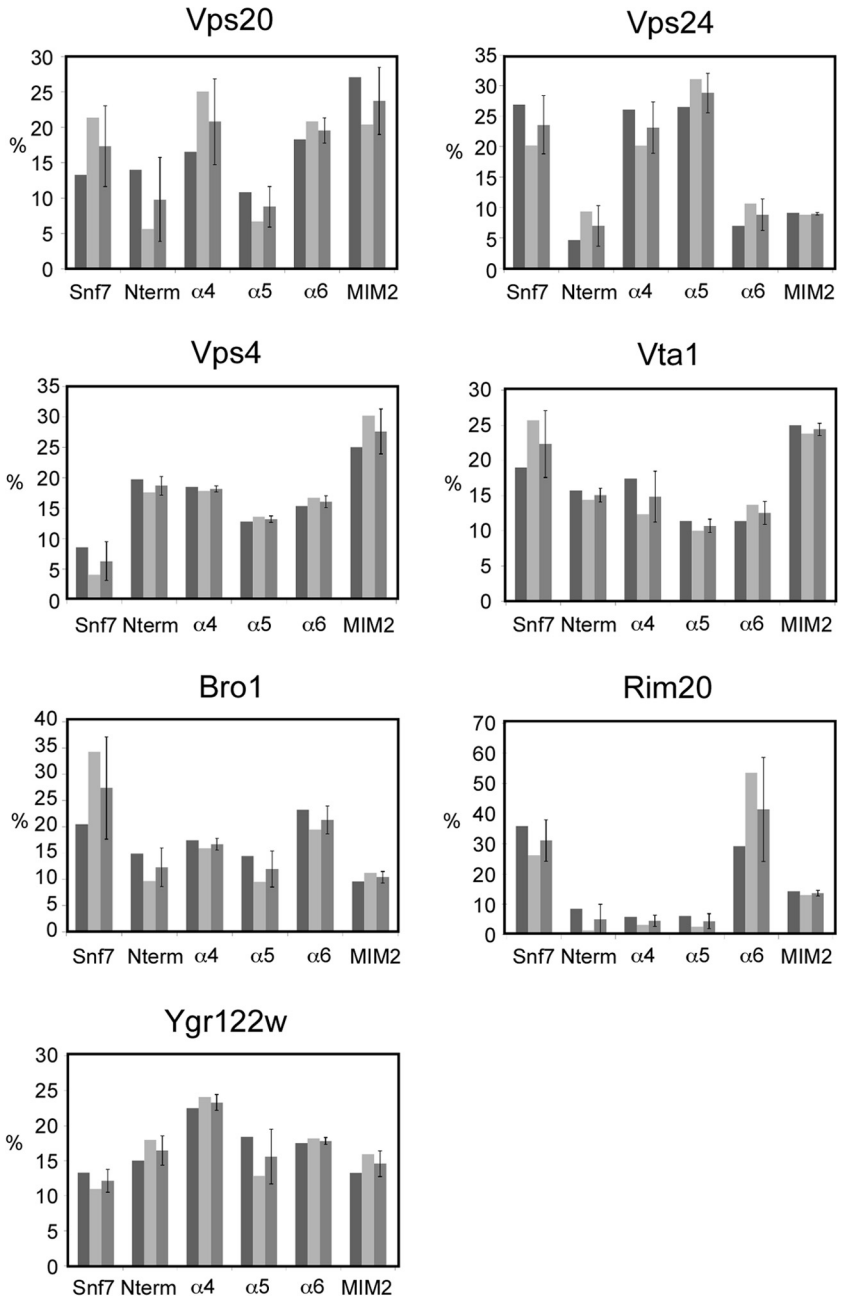

FIG 3 Quantification of the GST pulldown experiment. The Western blot signals in Fig. 2 were quantified using the program ImageJ. The panels summarize the results obtained with each binding partner. The binding partner studied is indicated above each panel. For the whole set of GST fusions, the binding intensities measured in one experiment with a specific interaction partner were summed up and set to 100%. In each panel, the degree of binding to the different GST fusions (as a percent of the total) is presented. For each GST fusion, three columns are shown: the left and middle columns show the results of two independent sets of experiments, and the right column shows the average of these two experiments with the standard deviation.

and spun in a centrifuge. Due to their low density, membranes float to the top of the gradient. Fractions were collected from the gradient and examined for the presence of Snf7 by Western blotting. About 21% of wild-type Snf7, compared to 73% of Snf7Δα6, was found in the membrane fractions (top 3 fractions) (Fig. 8). These values are in excellent agreement with our differential centrifugation experiment. These experiments show that Snf7Δα6 retains the ability to associate with (presumably endosomal) membranes and that the membrane-associated fraction is much greater than in the case of wild-type Snf7. This could indicate that Snf7Δα6 is defective for removal from the endosomal membrane by the Vps4 ATPase complex.

DISCUSSION

We established binding profiles along the Snf7 sequence for different Snf7 binding partners. With different binding partners, distinct profiles were observed. The main interactions are depicted in Fig. 9A.

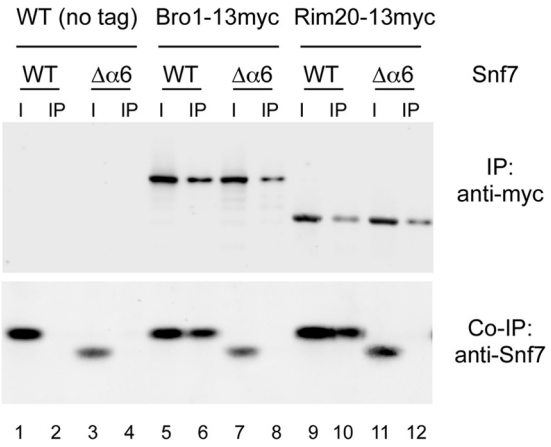

FIG 4 Effect of the α6 deletion on Bro1 and Rim20 binding *in vivo*. Binding was analyzed by coimmunoprecipitation. Different *SNF7* deletion strains were transformed with plasmids expressing either wild-type *SNF7* (pRK861) or the *snf7*Δα6 deletion mutant (pRK1487). 13myc-tagged proteins were precipitated from cell extracts with anti-Myc antibodies (9E10) and analyzed by Western blotting with anti-Myc antibodies (top) or anti-Snf7 antibodies (bottom). Lanes 1 to 4, RKY2673 (Δ*snf7*); lanes 5 to 8: RKY2030 (*BRO1-13myc*); lanes 9 to 12, RKY2097 (*RIM20-13myc*). Lanes 1, 2, 5, 6, 9, and 10, pRK861; lanes 3, 4, 7, 8, 11, and 12, pRK1487. Odd-numbered lanes show input (I; anti-Myc blot, 10%; anti-Snf7 blot, 1%); even-numbered lanes show immunopreciptation (IP) results.

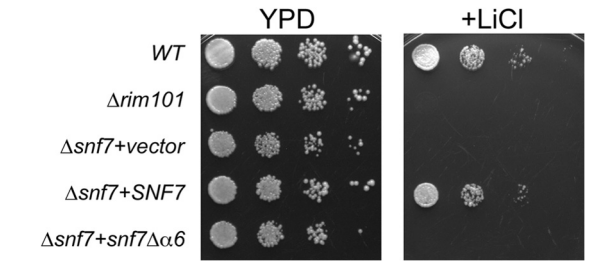

FIG 6 LiCl sensitivity of the *snf7*Δα6 mutant. To test for LiCl sensitivity, 10-fold serial dilutions of different cultures were spotted onto YPD plates (left) and YPD plates containing 0.3 M LiCl (right). Plates were incubated for 3 days at 30°C. Strains (top to bottom): JD52 (wild type [WT]), RKY2175 (Δ*rim101*), RKY2673/YCplac33 (Δ*snf7*), RKY2673/pRK861 (*SNF7*), and RKY2673/pRK1487 (*snf7*Δα6).

Unraveling the precise molecular architecture of the ESCRT-III complex is challenging, and despite substantial progress, information about the dynamics of the intramolecular interactions within the complex is still limited. It has been suggested that ESCRT-III subunits are present in a "closed" conformation in solution, which prevents homo- or heterooligomerization (32). In the closed state, the α5-α6 region is thought to interact with the α2 helix. Upon membrane binding, a transition from the closed to the open state occurs by an unknown mechanism. In the open state, oligomerization may take place. Vps20 seems to play a role in nucleating Snf7 oligomerization, while Vps24 is instead involved in disassembly of Snf7 oligomers (11, 12). The complementary binding profiles for the ESCRT-III subunits Vps20 and Vps24 now suggest a model for the events occurring during an assembly-disassembly cycle of ESCRT-III at the vacuolar membrane. Accordingly, through its strong binding to the MIM2-α6 region, Vps20 could relieve Snf7 autoinhibition and convert it to the oligomerization proficient open conformation. Vps24, in turn, competes with Vps20 for Snf7 binding through its strong α4-α5 interaction, thus replacing Vps20 in the Snf7 oligomer. Now the MIM2 region is free to interact with the Vps4-Vta1 complex, which ultimately leads to disassembly of ESCRT-III.

In this context, it is noticeable that Vps4 and Vta1 differed in their binding to full-length Snf7. Vps4 bound much better to the MIM2 fragment than to full-length Snf7, while Vta1 showed the same degree of binding in both cases. It is reasonable to assume

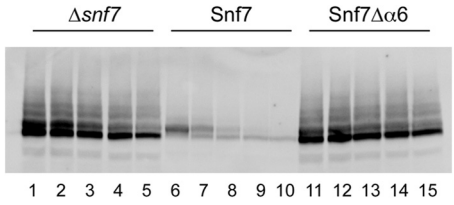

FIG 5 Effect of the α6 deletion on Ste6 turnover. Ste6 turnover was analyzed by Gal depletion. The *SNF7* deletion strain RKY2673 was transformed with the vector plasmid YCplac33 (lanes 1 to 5) or with plasmids expressing either wild-type *SNF7* (pRK861) (lanes 6 to 10) or the *snf7*Δα6 deletion mutant (pRK1487) (lanes 11 to 15) and with plasmid pRK505 carrying *STE6-myc* under the control of the *GAL1* promoter. Cells were grown to exponential phase in galactose medium and were then shifted to glucose-containing medium at time zero. Aliquots were taken at 20-min intervals and analyzed for the presence of Ste6-Myc by Western blotting with anti-Myc antibodies.

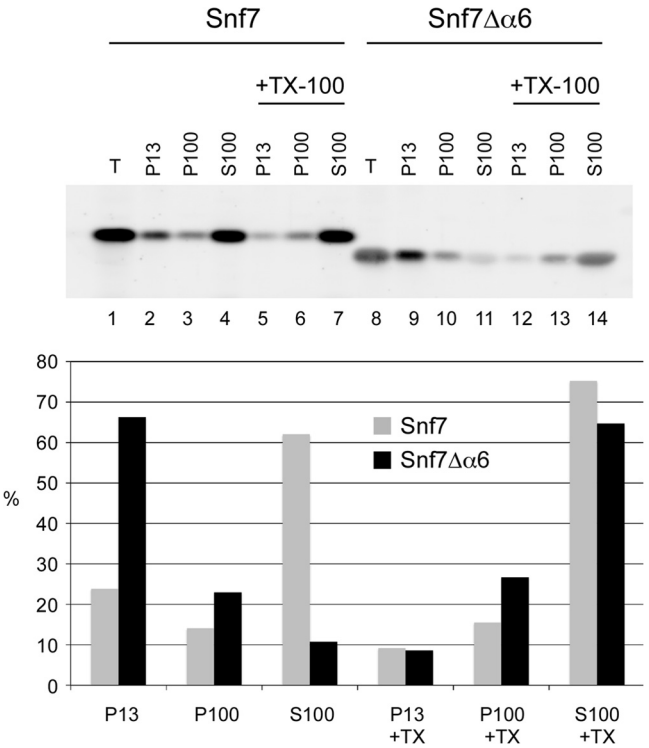

FIG 7 Fractionation of Snf7 by differential centrifugation. Strains RKY2673/pRK861 (WT Snf7) (lanes 1 to 7) and RKY2673/pRK1487 (Snf7Δα6) (lanes 8 to 14) were fractionated by differential centrifugation. Lanes 1 and 8, total fractions; lanes 2, 5, 9, and 12, P13 pellet; lanes 3, 6, 10, and 13, P100 pellet; lanes 4, 7, 11, and 14, S100 soluble fraction. Half of the cell extract was treated with 1% Triton X-100 before fractionation (lanes 5 to 7 and 12 to 14). (Top) Western blot with anti-Snf7 antibodies; (bottom) quantification of the Western blot signals with ImageJ (P13 + P100 + S100 = 100%).

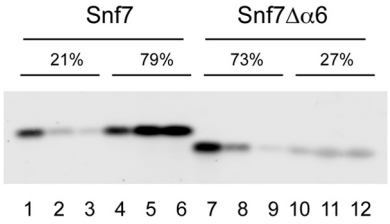

FIG 8 Analysis of membrane association by flotation. Cell extracts of RKY2673/pRK861 (WT Snf7) (lanes 1 to 6) and RKY2673/pRK1487 (Snf7Δα6) (lanes 7 to 12) were analyzed by flotation. Six equal fractions were collected from the flotation gradient. The top three fractions (lanes 1 to 3 and 7 to 9) correspond to the membrane fraction. The fractions were analyzed by Western blotting with anti-Snf7 antibodies. The amounts of Snf7 protein present in the top three fractions and the lower three fractions are indicated.

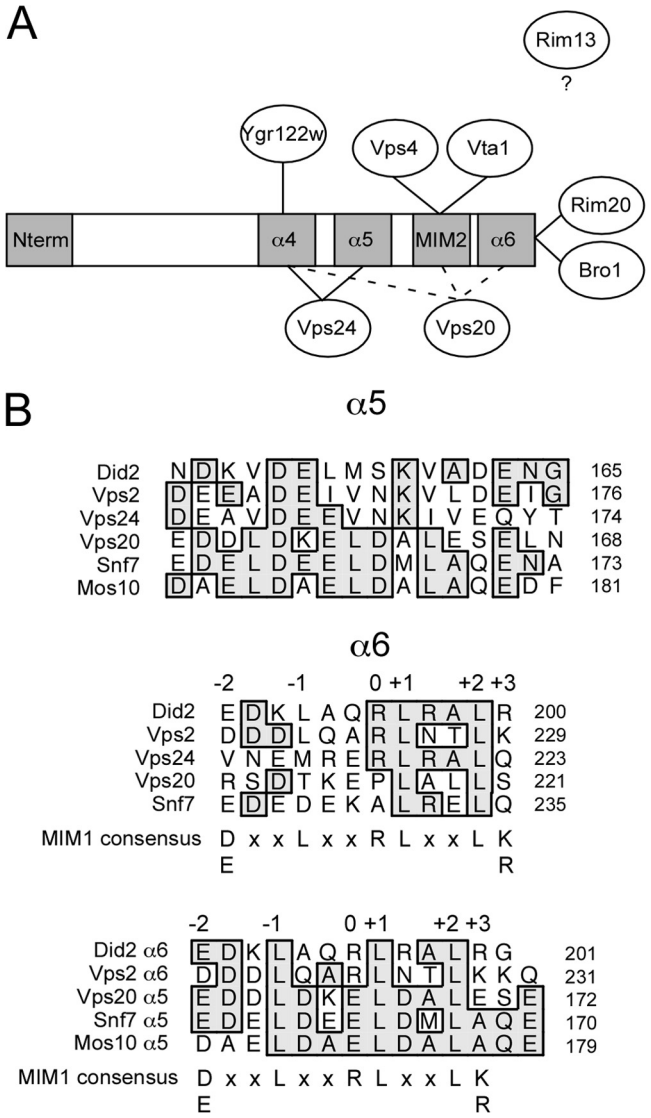

FIG 9 Snf7 interaction map and potential MIM motifs in the α5 and α6 helices of ESCRT-III family proteins. (A) Summary of the main interactions identified by our *in vitro* binding study between the Snf7 binding partners and binding motifs in Snf7. (B) Alignment of the α5 helices of the yeast ESCRT-III family proteins (top), alignment of the α6 helices with the MIM1 consensus sequence (middle), and a mixed alignment of α5 and α6 helices of ESCRT-III family proteins with MIM1 consensus sequence (bottom). The arginine residue in the middle of the sequence (position 0) serves as a reference point.

that Snf7 expressed in *E. coli* is present in its closed conformation. From our findings, we therefore conclude that Vps4 is not able to bind to the closed conformation of Snf7. This is in line with a previous study in which no interaction between purified Vps4 and Snf7 could be detected *in vitro*, while *in vivo* data clearly pointed to a direct interaction between Vps4 and Snf7 (14). The only evidence so far for a Snf7-Vta1 interaction stems from two-hybrid data (13). Although we detected binding of Vta1 to full-length Snf7 and to Snf7 fragments, this interaction could be indirect. Vta1 exists in a complex with Vps4, and there is good evidence that Vps4 directly binds to Snf7. Thus, Vta1 could bind to Snf7 indirectly as part of the Vps4-Vta1 complex. However, this does not seem to be the case, since Vps4 hardly binds to full-length Snf7 under the conditions of our experiment, while Vta1 shows a robust binding signal. However, binding could be mediated by other components of the ESCRT machinery. Evidence has been presented that Did2 is required for the Snf7-Vta1 interaction (33).

Our findings further suggest that Vta1 is able to bind to the "closed" conformation of Snf7. A similar conclusion was reached for the interaction between human VTA1 and LIP5, the human orthologue of the yeast ESCRT-III associated protein Mos10/Vps60 (34). Interestingly, LIP5/Mos10 does not possess an α6 helix, instead, VTA1 binds to the α5 helix of LIP5. A well-documented interaction between ESCRT-III proteins and Vps4 is the MIM1-MIT domain interaction (15, 16). However, a MIM1 consensus sequence is found in the α6 helices of only Did2 and Vps2, not in the other members of the ESCRT-III family. But, upon closer inspection of the α5 and α6 sequences, we noticed that the α5 sequences of the remaining ESCRT-III or ESCRT-III-like proteins (Snf7, Vps20, and Mos10/Vps60) closely resemble in their structure the MIM1 motif (Fig. 9B). They show the same spacing of leucine residues (at position −1, +1, and + 2) and have an acidic residue at position −2. The only difference is that negatively charged residues replace the positively charged residues at position 0 and + 3. We therefore propose that the α5 helices of these ESCRT-III proteins contains a MIM1 variant motif. This motif would be well suited for binding to the Vta1 MIT domains, since these domains show a different charge distribution in the MIM1 binding pocket than the Vps4 MIT domain (20). However, under the conditions of our experiment, this does not seem to be the preferred interaction between Snf7 and Vta1. Similar to Vps4, Vta1 rather seems to interact mainly with the MIM2 motif in Snf7.

The Bro domain proteins Bro1, Rim20, and Ygr122w displayed different profiles of binding to the Snf7 fragments. This was somewhat unexpected, since in a previous study, it has been shown that the Bro1 domain interacts with the α6 helix of Snf7 (5). For Bro1, we could detect only a slight preference for α6. This suggests that other parts of Snf7 are also involved in the Bro1-Snf7 interaction. The finding that even when the Bro1-α6 interaction is disabled by mutation, some Snf7-dependent Bro1 binding to endosomal membranes can still be observed (5) supports this notion. Likewise, Ygr122w seems to bind to Snf7 through multiple interactions. In contrast, Rim20 showed a clear preference for the α6 helix. This finding is confirmed by our immunoprecipitation experiments, where Snf7Δα6 was no longer able to interact with Rim20. Thus, the α6 helix of Snf7 indeed appears to be the main site for interaction with Rim20.

The situation for Bro1 is less clear. Our *in vitro* binding studies argue for multiple interactions with Snf7, yet in the immunoprecipitation experiment, the interaction with Snf7 was completely abrogated by deletion of the α6 helix alone. A possible explanation could be that all the interactions detected *in vitro* do not occur at the same time but take place in a temporal order during a cycle of intraluminal vesicle formation and release. Our cell fractionation experiments suggest that Snf7Δα6 is trapped at a certain step in this cycle, presumably at or before the Vps4-dependent step. Evidence has been presented that Bro1 acts late in the ESCRT cycle at the intraluminal vesicle scission step (5, 19). Thus, some of the additional *in vitro* interactions that we observed may be relevant only after the block resulting from the α6 deletion.

Our experiments show that both Bro domain proteins, Bro1 and Rim20, bind to a common motif in Snf7. This is in line with previous findings that Bro1 and Rim20 compete for binding to Snf7 and that induction of the Rim pathway favors binding of Rim20 at the expense of Bro1 binding (35). Our functional analysis of the *snf7*Δα6 mutant further supports this contention in that both functions of Snf7 in MVB sorting and in Rim signaling are lost simultaneously by the α6 deletion, inasmuch as Snf7Δα6 appears to be still present in an ESCRT-III complex at the endosomal membrane and is thus potentially available for interaction with the downstream Rim components.

In our *in vitro* binding experiments, we observed interactions with most of the known Snf7 interaction partners, with the exception of Rim13, where no interaction could be detected. A possible explanation is suggested by recent findings that both Snf7 and Rim20 are required for Rim13 focus formation (36). If binding of Rim20 to Snf7 is necessary to stabilize the Rim13-Snf7 interaction, then possibly two different binding motifs are involved. Our GST pulldown assay, however, detects only one-to-one interactions and thus cannot reconstitute the trimeric complex. Due to the nature of our assay, other interactions that require additional reaction partners may also have been missed.

Altogether, our study highlights the network character of the ESCRT interactions. The view that the ESCRT cycle is governed by single one-to-one interactions between individual components may not be correct. Rather, many low-affinity interactions may contribute to the functional dynamics of the ESCRT complexes.

ACKNOWLEDGMENTS

We thank Thomas Brune for his help with some of the experiments.

This work was supported by DFG grant KO 963/5-2.

REFERENCES

1. **Prescianotto-Baschong C, Riezman H.** 2002. Ordering of compartments in the yeast endocytic pathway. Traffic **3:**37–49.
2. **Maxfield FR, McGraw TE.** 2004. Endocytic recycling. Nat. Rev. Mol. Cell Biol. **5:**121–132.
3. **Odorizzi G, Babst M, Emr SD.** 1998. Fab1p PtdIns(3)P 5-kinase function essential for protein sorting in the multivesicular body. Cell **95:**847–858.
4. **Henne WM, Buchkovich NJ, Emr SD.** 2011. The ESCRT pathway. Dev. Cell **21:**77–91.
5. **Wemmer M, Azmi I, West M, Davies B, Katzmann D, Odorizzi G.** 2011. Bro1 binding to Snf7 regulates ESCRT-III membrane scission activity in yeast. J. Cell Biol. **192:**295–306.
6. **Wollert T, Hurley JH.** 2010. Molecular mechanism of multivesicular body biogenesis by ESCRT complexes. Nature **464:**864–869.
7. **Babst M, Katzmann DJ, Estepa-Sabal EJ, Meerloo T, Emr SD.** 2002. ESCRT-III: an endosome-associated heterooligomeric protein complex required for MVB sorting. Dev. Cell **3:**271–282.
8. **Howard TL, Stauffer DR, Degnin CR, Hollenberg SM.** 2001. CHMP1 functions as a member of a newly defined family of vesicle trafficking proteins. J. Cell Sci. **114:**2395–2404.
9. **Kranz A, Kinner A, Kölling R.** 2001. A family of small coiled-coil-forming proteins functioning at the late endosome in yeast. Mol. Biol. Cell **12:**711–723.
10. **Amerik AY, Nowak J, Swaminathan S, Hochstrasser M.** 2000. The Doa4 deubiquitinating enzyme is functionally linked to the vacuolar protein-sorting and endocytic pathways. Mol. Biol. Cell **11:**3365–3380.
11. **Saksena S, Wahlman J, Teis D, Johnson AE, Emr SD.** 2009. Functional reconstitution of ESCRT-III assembly and disassembly. Cell **136:**97–109.
12. **Teis D, Saksena S, Emr SD.** 2008. Ordered assembly of the ESCRT-III complex on endosomes is required to sequester cargo during MVB formation. Dev. Cell **15:**578–589.
13. **Bowers K, Lottridge J, Helliwell SB, Goldthwaite LM, Luzio JP, Stevens TH.** 2004. Protein-protein interactions of ESCRT complexes in the yeast *Saccharomyces cerevisiae*. Traffic **5:**194–210.
14. **Shestakova A, Hanono A, Drosner S, Curtiss M, Davies BA, Katzmann DJ, Babst M.** 2010. Assembly of the AAA ATPase Vps4 on ESCRT-III. Mol. Biol. Cell **21:**1059–1071.
15. **Obita T, Saksena S, Ghazi-Tabatabai S, Gill DJ, Perisic O, Emr SD, Williams RL.** 2007. Structural basis for selective recognition of ESCRT-III by the AAA ATPase Vps4. Nature **449:**735–739.
16. **Stuchell-Brereton MD, Skalicky JJ, Kieffer C, Karren MA, Ghaffarian S, Sundquist WI.** 2007. ESCRT-III recognition by VPS4 ATPases. Nature **449:**740–744.
17. **Kieffer C, Skalicky JJ, Morita E, De Domenico I, Ward DM, Kaplan J, Sundquist WI.** 2008. Two distinct modes of ESCRT-III recognition are required for VPS4 functions in lysosomal protein targeting and HIV-1 budding. Dev. Cell **15:**62–73.
18. **Richter C, West M, Odorizzi G.** 2007. Dual mechanisms specify Doa4-mediated deubiquitination at multivesicular bodies. EMBO J. **26:**2454–2464.
19. **Nikko E, André B.** 2007. Evidence for a direct role of the Doa4 deubiquitinating enzyme in protein sorting into the MVB pathway. Traffic **8:**566–581.
20. **Xiao J, Xia H, Zhou J, Azmi IF, Davies BA, Katzmann DJ, Xu Z.** 2008. Structural basis of Vta1 function in the multivesicular body sorting pathway. Dev. Cell **14:**37–49.
21. **Hayashi M, Fukuzawa T, Sorimachi H, Maeda T.** 2005. Constitutive activation of the pH-responsive Rim101 pathway in yeast mutants defective in late steps of the MVB/ESCRT pathway. Mol. Cell. Biol. **25:**9478–9490.
22. **Rothfels K, Tanny JC, Molnar E, Friesen H, Commisso C, Segall J.** 2005. Components of the ESCRT pathway, *DFG16*, and *YGR122w* are required for Rim101 to act as a corepressor with Nrg1 at the negative regulatory element of the *DIT1* gene of *Saccharomyces cerevisiae*. Mol. Cell. Biol. **25:**6772–6788.
23. **Xu W, Smith FJ, Jr, Subaran R, Mitchell AP.** 2004. Multivesicular body-ESCRT components function in pH response regulation in *Saccharomyces cerevisiae* and *Candida albicans*. Mol. Biol. Cell **15:**5528–5537.
24. **Wolf JM, Davis DA.** 2010. Mutational analysis of Candida albicans *SNF7* reveals genetically separable Rim101 and ESCRT functions and demonstrates divergence in bro1-domain protein interactions. Genetics **184:**673–694.
25. **Li W, Mitchell AP.** 1997. Proteolytic activation of Rim1p, a positive regulator of yeast sporulation and invasive growth. Genetics **145:**63–73.
26. **Ito T, Chiba T, Ozawa R, Yoshida M, Hattori M, Sakaki Y.** 2001. A comprehensive two-hybrid analysis to explore the yeast protein interactome. Proc. Natl. Acad. Sci. U. S. A. **98:**4569–4574.
27. **Weiss P, Huppert S, Kölling R.** 2009. Analysis of the dual function of the ESCRT-III protein Snf7 in endocytic trafficking and in gene expression. Biochem. J. **424:**89–97.
28. **Xu W, Mitchell AP.** 2001. Yeast PalA/AIP1/Alix homolog Rim20p associates with a PEST-like region and is required for its proteolytic cleavage. J. Bacteriol. **183:**6917–6923.
29. **Longtine MS, McKenzie A, Demarini DJ, Shah NG, Wach A, Brachat A, Philippsen P, Pringle JR.** 1998. Additional modules for versatile and economical PCR-based gene deletion and modification in *Saccharomyces cerevisiae*. Yeast **14:**953–961.
30. **Muziol T, Pineda-Molina E, Ravelli RB, Zamborlini A, Usami Y, Göttlinger H, Weissenhorn W.** 2006. Structural basis for budding by the ESCRT-III factor CHMP3. Dev. Cell **10:**821–830.
31. **McCullough J, Fisher RD, Whitby FG, Sundquist WI, Hill CP.** 2008. ALIX-CHMP4 interactions in the human ESCRT pathway. Proc. Natl. Acad. Sci. U. S. A. **105:**7687–7691.

32. **Shim S, Kimpler LA, Hanson PI.** 2007. Structure/function analysis of four core ESCRT-III proteins reveals common regulatory role for extreme C-terminal domain. Traffic **8:**1068–1079.
33. **Lottridge JM, Flannery AR, Vincelli JL, Stevens TH.** 2006. Vta1p and Vps46p regulate the membrane association and ATPase activity of Vps4p at the yeast multivesicular body. Proc. Natl. Acad. Sci. U. S. A. **103:**6202–6207.
34. **Shim S, Merrill SA, Hanson PI.** 2008. Novel interactions of ESCRT-III with LIP5 and VPS4 and their implications for ESCRT-III disassembly. Mol. Biol. Cell **19:**2661–2672.
35. **Boysen JH, Mitchell AP.** 2006. Control of Bro1-domain protein Rim20 localization by external pH, ESCRT machinery, and the *Saccharomyces cerevisiae* Rim101 pathway. Mol. Biol. Cell **17:**1344–1353.
36. **Subramanian S, Woolford CA, Desai JV, Lanni F, Mitchell AP.** 2012. *cis*- and *trans*-acting localization determinants of pH response regulator Rim13 in *Saccharomyces cerevisiae*. Eukaryot. Cell **11:**1201–1209.